Biophysical Chemistry, 32 (1988) 187–198
Elsevier

BPC 01324

Time-resolved emission spectra of hemoglobin on the picosecond time scale

Enrico Bucci, Henryk Malak, Clara Fronticelli, Ignacy Gryczynski, Gabor Laczko and Joseph R. Lakowicz

Department of Biological Chemistry, University of Maryland, School of Medicine, 660 W. Redwood Street, Baltimore, MD 21201, U.S.A.

Received 20 June 1988
Revised manuscript received 14 September 1988
Accepted 14 September 1988

Hemoglobin; Tryptophan fluorescence; Picosecond spectroscopy; Time-resolved emission

We used front-face illumination to examine the steady-state and time-resolved emission from the intrinsic tryptophan emission of human hemoglobin (Hb). Experimental conditions were identified which eliminated all contributions of scattered light. The sensitivity obtained using front-face optics was adequate to allow measurement of the wavelength-dependent frequency response of the emission to 2 GHz. The intensity decays displayed pico- and nanosecond components in the emission at all wavelengths from 315 to 380 nm. The contribution of the picosecond component decreased from 72 to 37% over this range of wavelengths. Frequency-domain measurements were used to calculate the time-resolved emission spectra and decay-associated emission spectra. These spectra indicate that the picosecond components of the emission display maxima near 320 nm, whereas the nanosecond components are centered at longer wavelengths near 335 nm. The nanosecond components appear to be due to residual impurities which remain even in highly purified samples of Hb. However, we cannot eliminate the possibility that some of these components are due to Hb itself.

1. Introduction

The intrinsic tryptophan emission from proteins has been widely used to examine their conformation and dynamics [1–4]. However, the intrinsic fluorescence of hemoglobin (Hb) has only been studied infrequently because this emission is strongly quenched by energy transfer to the heme [5–7]. Because the tryptophan emission from heme proteins is 100–10000-fold weaker than that of nonheme proteins, the emission from even a small percentage of nonheme impurities can dominate the emission from Hb samples. For the same reason, the intensity of Raman and Rayleigh scattered light, and of stray light, may become a major component of the detected signal, producing meaningless data.

Because of the high efficiency of tryptophan-to-heme energy transfer, one expects the tryptophan decay times to be in the picosecond time range. In fact, picosecond components in the intensity decay of Hb have been detected in three laboratories [8–10]. In all cases these laboratories also reported the existence of nanosecond components. While the preexponential factors of the picosecond components exceeded 99%, the relative intensity of these components was typically 30–45% of the total emission. The origin of these longer-lived decays is uncertain. The nanosecond decay times indicate either that there are conformations of the Hb molecules in which the transfer of energy from the tryptophans is inhibited, or that these components are due to impurities.

In the present paper, we describe experimental conditions by which one can eliminate the contri-

Correspondence address: J.R. Lakowicz, Department of Biological Chemistry, University of Maryland, School of Medicine, 660 W. Redwood Street, Baltimore, MD 21201, U.S.A.

Abbreviations: Hb, hemoglobin, HbO_2, oxyhemoglobin, HbCO, carbonmonoxyhemoglobin; apohemoglobin, heme-free hemoglobin; DAS, decay-associated emission spectra; χ^2_R, reduced chi-square.

bution of scattered or stray light to the signals detected from optically dense solutions of Hb. We use illumination and observation from the front surface of the samples, as suggested by Eisinger and Flores [11], and as pioneered for studies of Hb fluorescence of Hirsch and colleagues [12,13]. The picosecond components persist even after careful elimination of scattered light. The nanosecond components also persist, but appear to decrease in amplitude with additional purification. The picosecond components emit at shorter wavelengths, and these components do not appear to relax to longer wavelengths. This suggests, but does not prove, that the nanosecond components are due to impurities.

2. Materials and methods

Human Hb was prepared from washed red cells, obtained from fresh blood samples donated by the local blood bank. They were hemolyzed in 0.005 M phosphate buffer at pH 7.0 and the stromata were eliminated by treatment of the solutions with 10 g/dl of chloroform. If necessary, the protein was concentrated up to 10% by ultrafiltration through a 10 kDa pellicon cassette, dialyzed vs. water, recycled through a mixed-bed resin cartridge for removing polyphosphates and other ions, and stored at $-90\,^{\circ}$C.

Oxyhemoglobin (HbO_2) was purified by HPLC through a DEAE 5PW preparative column using a gradient formed by 0.015 M Tris-acetate at pH 8, and 0.015 M Tris-acetate at pH 7.7 with 0.2 M sodium acetate. All measurements were conducted at 4° C in the buffer as eluted from the column. Protein concentration was measured spectrophotometrically using $E = 0.868$ cm^2 mg^{-1} for the carbonmonoxy derivative at 540 nm. Absorbances were measured using a Cary 14 spectrophotometer.

Spectroscopic fluorescence measurements were performed using front-face optical conditions. A triangular cuvette was positioned so that the incident beam was at 34° from the normal to the reflecting surface. This orientation was found to provide 10% higher intensities than an angle of 56°. The protein concentration was kept at 20 mg/ml. At this concentration and above, the intensity of emission was independent of protein concentration, indicating total absorption of the incident light.

Steady-state fluorescence measurements were carried out with an SLM 8000 photon-counting spectrofluorometer. Lifetimes and correlation times were measured using a frequency-domain fluorometer operating between 8 and 2000 MHz [14]. The modulated excitation was provided by the harmonic content of a laser pulse train with a repetition rate of 3.75 MHz and a pulse width of 5 ps, from a synchronously pumped and cavity-dumped rhodamine 6G dye laser. The dye laser was pumped with a mode-locked argon ion laser (Coherent, Innova 15). The dye laser output was frequency-doubled to 290 nm with an angle-tuned KDP crystal. The emitted light was observed with a microchannel photomultiplier (Hamamatsu R1564U), and the cross-correlation detection was performed outside the photomultiplier tube [14]. The emission was observed either through a combination of broad-band emission filters [10], or through 10 nm bandpass interference filters. For intensity decay measurements, magic-angle polarizer orientations were used.

The frequency-domain data were used to recover the intensity decays

$$I(\lambda,t) = \sum_i \alpha_i(\lambda) e^{-t/\tau_i} \tag{1}$$

where $\alpha_i(\lambda)$ are the preexponential factors, τ_i the decay times (which are assumed to be independent of wavelength), and λ the emission wavelength. The contribution of each component to the total (steady-state) emission is given by

$$f_i(\lambda) = \frac{\alpha_i(\lambda)\tau_i}{\sum_i \alpha_i(\lambda)\tau_i} \tag{2}$$

The phase and modulation data from 8 MHz to 2 GHz were used to recover the intensity decay at each wavelength, or globally across the emission spectra, as described previously [15].

The impulse response functions (eq. 1) can be used to calculate time-resolved emission spectra and emission centers-of-gravity [16–18]. This re-

quires normalization of the preexponential factors, so the integrated intensity represents the steady-state intensity $F(\lambda)$ at each wavelength. Normalization is accomplished using the factor $H(\lambda)$ which is calculated using

$$H(\lambda) = \frac{F(\lambda)}{\int_0^\infty I(\lambda,t)\,dt} \tag{3}$$

$$= \frac{F(\lambda)}{\alpha_1(\lambda)\tau_1 + \alpha_2(\lambda)\tau_2 + \alpha_3(\lambda)\tau_3} \tag{4}$$

Then, the appropriately normalized functions are given by

$$I'(\lambda,t) = H(\lambda)I(\lambda,t) \tag{5}$$

$$= \sum_i \alpha_i'(\lambda)e^{-t/\tau_i} \tag{6}$$

where $\alpha_i'(\lambda) = H(\lambda)\alpha_i(\lambda)$. For any desired time ($t_i$), the time-resolved emission spectrum is obtained by plotting the values $I'(\lambda,t_i)$.

The time-dependent spectral shifts can be characterized by the time-dependent center of gravity, in wave numbers (cm^{-1} or $kK = 10^3\,cm^{-1}$), which is proportional to the average energy of the emission. Our data were collected at approximately equally spaced wavelength intervals. For these conditions [17], the center of gravity in kK is given by:

$$\bar{\nu}_{cg}(t) = 10000\frac{\sum_\lambda I'(\lambda,t)\lambda^{-1}}{\sum_\lambda I'(\lambda,t)} \tag{7}$$

The time-dependent spectral width ($\Delta\bar{\nu}_{cg}(t)$) can be revealing with regard to the nature of the time-dependent spectral shifts. For instance, in the case of time-dependent solvent relaxation the time-dependent width can reveal whether the emission spectrum shifts toward longer wavelength without changes in shape (continuous relaxation), or whether there are two or more emitting states formed during relaxation (stepwise relaxation). In these cases the spectral width either remains constant or increases transiently, respectively [17]. In the presence of impurity contributions to the emission, or equivalently a mixture of emitting species, it seems that the values of $\Delta\bar{\nu}_{cg}(t)$ will be characteristic of the shortest component at $t = 0$, (if the α_i value of the short component is dominant), and of the longest emitting species at longer times. Hence, $\Delta\bar{\nu}_{cg}(t)$ is expected to be time-dependent, but the value can increase or decrease depending upon the emission spectra of the emitting species. The time-dependent half-widths were calculated using

$$\Delta\bar{\nu}_{cg}(t) = \frac{\sum_\lambda \left(10000/\lambda - \bar{\nu}_{cg}(t)\right)^2 I'(\lambda,t)}{\sum_\lambda I'(\lambda,t)}. \tag{8}$$

where λ is in nm. The time-resolved emission can also be visualized by the decay-associated spectra (DAS), as suggested by Brand and co-workers [29,30]. These are the emission spectra which are associated with each decay time ($I_i(\lambda)$). The DAS are given by

$$I_i(\lambda) = f_i(\lambda)F(\lambda) \tag{9}$$

where $F(\lambda)$ is the steady-state emission spectrum and $f_i(\lambda)$ the fractional intensity of the i-th component as defined by eq. 2.

3. Results and discussion

We previously reported the use of 2 GHz frequency-domain fluorometry to detect three decay times for the intrinsic tryptophan emission of Hb, with decay times ranging from 15 ps to 8 ns [10]. The shortest components were near 9, 14, and 27 ps in deoxy-, oxy- and carbonmonoxyhemoglobin, respectively. The preexponential factors of the lifetimes indicated that between 98.8 and 99.2% of the emission at short times (< 25 ps) was due to the components which displayed the picosecond decay times. Nonetheless, the contribution of these components to the total (steady-state) intensity was only 30–45%, due to their short lifetimes. Thus, the steady-state emission spectra were largely dominated by the emission in the nanosecond range. In these studies we used right-

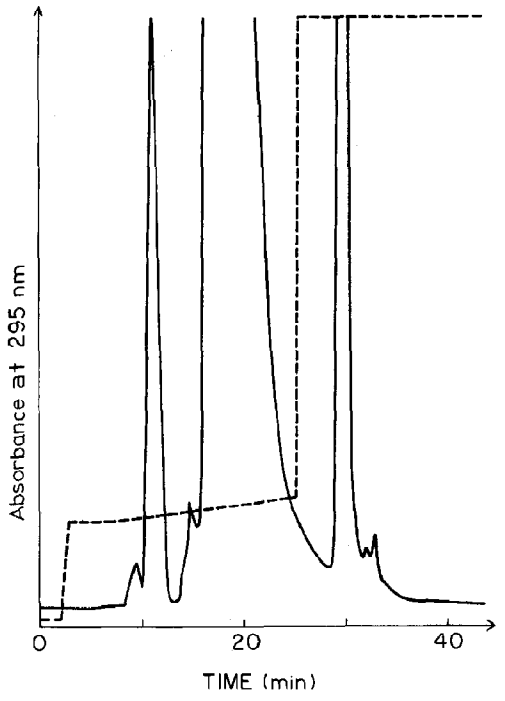

Fig. 1. HPLC elution profile of Hb on a DEAE 5PW column. The gradient was obtained with 0.015 M Tris buffer at pH 8.0 and 0.015 M Tris buffer at pH 7.7 with 0.2 M sodium acetate. Abscissa: absorbance measured at 295 nm. The dashed line represents the percentage of the second buffer in the gradient, from 0 to 100%.

angle optics, and it was therefore necessary to use concentrations of Hb near 0.2 mg/ml. At these concentrations the Hb molecules would be partially dissociated into dimers, probably to an extent near 10%. In order to clarify the origins of the picosecond and nanosecond components, we examined the emission spectra, anisotropies and frequency responses at higher concentrations, which required the use of front-face optics.

On the assumption that the nanosecond emitters were non-Hb impurities, we first refined the chromatographic procedure, eventually adopting the gradient shown in fig. 1. The main fraction was isolated and identified as hemoglobin A_0 by electrophoresis. Table 1 shows the intensity decay measured from Hb samples purified by this column and gradient. In this experiment square geometry was used, in conjunction with filters to eliminate the Raman and Rayleigh scattering of the samples [10]. More than 50% of the emitted light was sacrificed to the filters (see fig. 2 of ref. 10). The preexponentials showed that 99.8% of the initial intensity was due to the picosecond components. However, because of their longer decay times, the nanosecond components with α_i values of less than 0.01 still contributed 20–30% to the total (steady-state) intensity. In the present measurements, the nanosecond components contributed less to the intensity decay than in our earlier studies (table 1 of ref. 10), which is consistent with the presence of impurities. This allowed a better resolution of the picosecond lifetimes from the nanosecond components.

It is important to recognize the physical meaning of the $\alpha_i(\lambda)$ values, and how these values can be interpreted in the case of heme and nonheme proteins. In the present system the emission is almost certainly due to tryptophan residues, which will display the same radiative (emission) rate, irrespective of energy transfer to the heme, and irrespective of other quenching processes. Since the observed emission is proportional to the emission rate, the value of $\alpha_i(\lambda)$ reflects the fractional population of each species with the associated lifetime. More specifically, one can state that the $\alpha_i(\lambda)$ value associated with the picosecond decay time reflects the fractional population of Hb molecules, and those associated with the two longer decay times reflect the fractional population of the nonheme emitters.

Table 1

Decay times of the tryptophan emission from hemoglobin

Sample [a]	τ_i (ns)	(S.D.) [b]	α_i	f_i	χ^2_R
HbO_2	0.015	(0.001)	0.995	0.700	
	0.902	(0.004)	0.004	0.195	
	7.640	(0.078)	0.003	0.103	1.95/ 25.83 [c]
HbCO [d]	0.025	(0.001)	0.994	0.683	
	1.048	(0.072)	0.005	0.139	
	7.385	(0.047)	0.001	0.177	1.72/ 27.26 [c]

[a] In 0.01 M phosphate buffer at pH 7.0 and 4° C; square geometry and filters as described in ref 10; excitation was at 295 nm; Hb concentration was 0.2 mg/ml.

[b] Obtained from the covariance matrix, or described by Bevington [28].

[c] The second value is the χ^2_R value from the two-decay-time fit.

In order to perform measurements at higher Hb concentrations, and to avoid ambiguities due to the dimer-tetramer equilibrium [19,20], we used front-face optics. Because of the weak emission of Hb we believe it is essential to delineate carefully the experimental conditions, emission spectra and control experiments used to demonstrate that the observed signals are in fact due to Hb.

The emission spectrum of HbO_2 at 2 g/dl is shown in fig. 2. In order to maximize the contribution of scattered light (worse-case conditions) both the excitation and emission were oriented vertically. In fig. 2 Rayleigh scatter and/or reflected light is the dominant component centered near 290 nm. The Hb emission is seen as a broad peak centered near 320 nm. We questioned whether Raman scatter or other stray light contributions were hidden under the Hb emission. Hence, we examined a solution of hemin, which is nonfluorescent, and which had an absorbance at 290 nm equivalent to that of our Hb sample. Additionally, we added Ludox until the scattering at 290 nm was 4-fold larger than that observed for the Hb sample. Even under these worse-case conditions, there were no spurious signals under the presumed Hb emission spectrum. As noted by Eisinger and

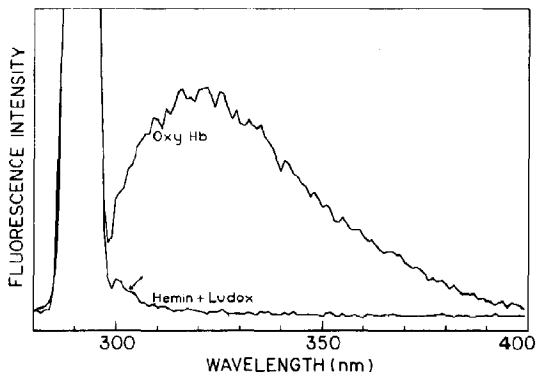

Fig. 2. Emission spectra recorded with vertically polarized front-face excitation at 290 nm. In order to maximize the scattering, the observation was through a vertically oriented polarizer. HbO_2 was in 0.015 M Tris buffer at pH 8.0, approx. 0.03 M sodium acetate, protein concentration 2 g/dl; hemin chloride was in 0.1 M NaOH with the absorption at 290 nm identical to that of HbO_2. The hemin was then titrated with Ludox until the scattering at 290 nm was 4-fold greater than that of HbO_2. The arrow indicates that the residual scattering of the hemin + Ludox sample is not significant above 300 nm.

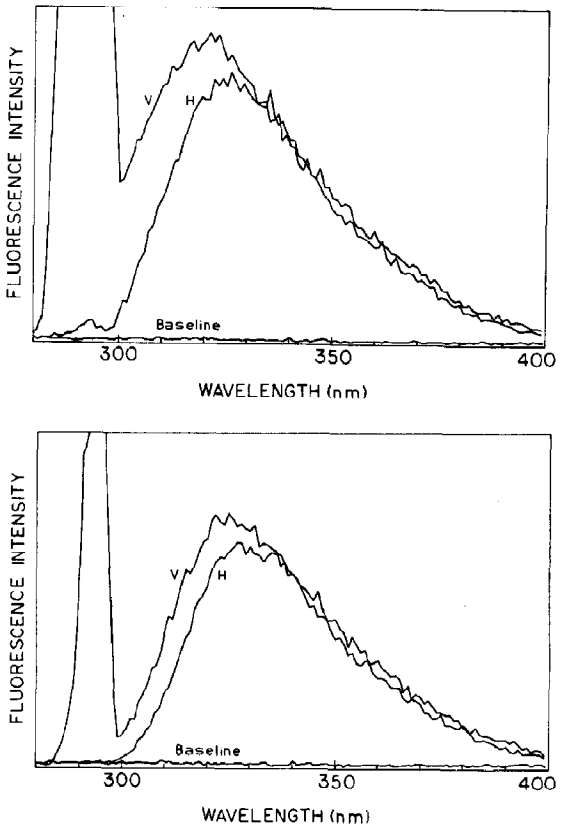

Fig. 3. Front-face emission spectra of HbO_2 under the same conditions as in fig. 2. (Top) Excitation at 290 nm, vertically polarized. The observation was through vertically (V) or horizontally (H) oriented polarizers. The lowest line shows the instrumental dark current. (Bottom) Same as top, except for a 10% cupric sulfate filter (2 mm thick) in the emission path.

Flores [11], Raman scatter, which is expected to occur off water near 320 nm, is not significant using front-face observation. Contributions of scattered and/or background signals are negligible above 300 nm. These spectra indicate that the Hb emission can be safely observed at any wavelength above 300 nm.

Additional emission spectra are shown in fig. 3. The contribution due to scattering at the excitation wavelength can be largely eliminated by use of an emission polarizer in the horizontal orientation (top). However, this approach is not useful for measurements of anisotropies, which require the use of two polarizer orientations, or lifetimes, which require the magic-angle orientation. Occa-

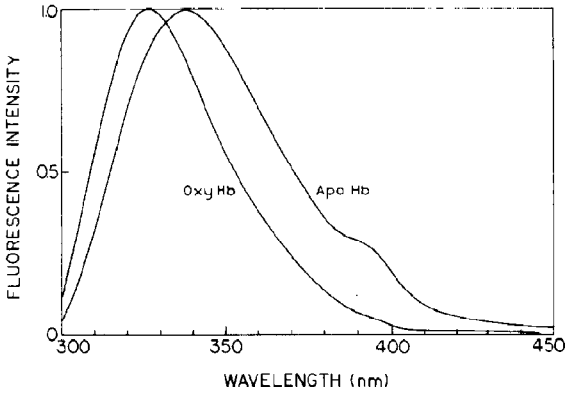

Fig. 4. Smoothed emission spectra of HbO_2 and apo-Hb under the same conditions as in fig. 3. In order to show better the narrowing of the spectral dispersion of oxyhemoglobin, the measurements were taken through a horizontal polarizer, which eliminated the scattering. The spectra are normalized. Square geometry and front-face fluorescence techniques were used for apo-Hb and HbO_2, respectively. The high transparency prevented the usage of front-face for apo-Hb. The usage of front-face eliminated the distortion of the spectrum of HbO_2 produced by the Raman scattering and by the inner-filter effect of the heme.

sionally, one needs to attenuate the intensity of the scattered light but not distort the shape of the emission spectrum. We found that this could be accomplished using a 10% solution of cupric sulfate, 2 mm thick (bottom). A 10% solution in the 2 mm path filter had 50% transmission at 305 nm and a transmission of 1% at 290 nm. Therefore, it reduced the intensity of the scattering, with only a small modification of the shape of the emission spectra.

The emission spectra shown in figs. 2 and 3 resulted from emissions whose intensity was distributed 70:30 between pico- and nanosecond lifetimes. They are characterized by a blue shift and a narrow dispersion compared to the emission spectra of heme-free (apo) Hb. This is clearly visible in fig. 4, which shows the superimposition of smoothed spectra of Hb and apo-Hb, where the Rayleigh scattering was totally eliminated by using a horizontal polarizer in the emission. The maximum intensity was at 320 nm in Hb and at 335 nm in apo-Hb. Also, visual inspection clearly indicates that the spectral dispersion of Hb was much narrower than that of apo-Hb. The blue shift may be expected on the basis of the short lifetimes that dominate the emission in that these emissions may result from tryptophan residues which are either not yet in equilibrium with their environment [18,21,22], or are shielded from the solvent by the protein matrix.

Further evidence for the absence of scattered light in the detected signals was obtained by measuring the anisotropy across the emission spectrum. The fluorescence anisotropy can be a reliable indicator of contribution due to scattered light. This is because the anisotropy, for randomly oriented fluorophores, cannot exceed 0.4 [23]. In contrast, scattered light is usually completely polarized, and its anisotropy is near 1.0. Hence, a small contribution of scattered light can be detected by anisotropies larger than 0.4, or for tryptophan larger than 0.32 [24]. In particular, if scattered light is significant then the anisotropy of the emission should be strongly dependent on wavelength, with higher anisotropy at the blue edge. The presence of Raman scatter would produce a peak in the anisotropy near 320 nm.

Wavelength-dependent anisotropies are shown for HbO_2 in fig. 5, with and without the cupric sulfate filter. The observations started at 305 nm, where the Rayleigh scattering was negligible. Identical data were obtained with and without the cupric sulfate filter in the emission path, which we take as additional evidence for the absence of Raleigh scattering. At 305 nm, the anisotropy of

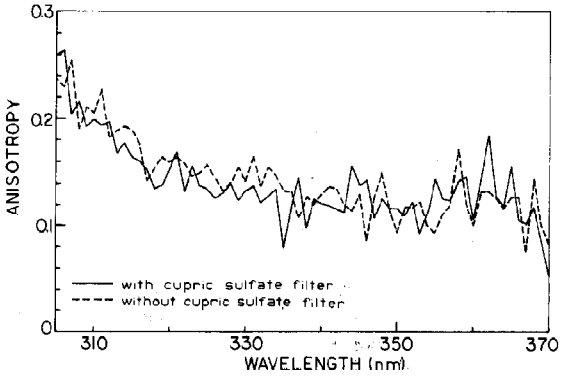

Fig. 5. Wavelength-dependent anisotropy of the emission from HbO_2 with (———) and without (— — —) the cupric sulfate emission filter.

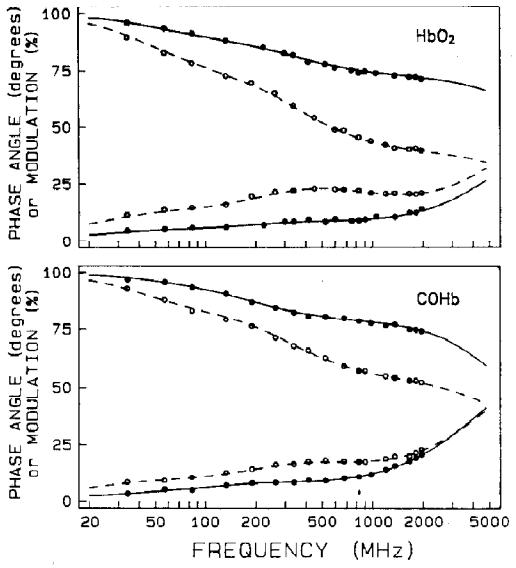

Fig. 6. Wavelength-dependent frequency response for HbO_2 (top) and HbCO (bottom). The symbols show the data at 315 (●) and 380 (○) nm. The solid lines show the best three-component fit to the data (tables 2 and 3).

the solutions was near 0.27, consistent with the frozen anisotropy of NATA [24,25], indicating the predominant presence at this wavelength of extremely short lifetimes. At longer wavelengths the anisotropy decreased to 0.1, consistent with the presence at these wavelengths of the longer lifetimes, in the nanosecond range. The above data collectively indicate that we can observe the emission of Hb from 310 to 370 nm, without significant contributions from scattered or stray light.

In order to calculate the time-resolved emission spectra it is necessary to measure the frequency response across the emission spectra. Typical data are shown in fig. 6, for the blue (315 nm) and red (380 nm) sides of the emission for HbO_2 (top) and HbCO (bottom). At each modulation frequency the phase angles are larger and the modulation smaller at 380 nm, relative to the measured values at 315 nm. This suggests longer mean decay times at the longer wavelengths, or alternatively, a larger contribution of the picosecond components at the shorter wavelengths.

The frequency responses were obtained at 315, 322, 340, 360 and 380 nm. At each wavelength they were analyzed individually to obtain the best three-decay-time fit. That is, the decay times were not held constant at all wavelengths. The goodness of the three-decay-time fits is evident from the good agreement between the data (●, ○) and the calculated curves (fig. 6). Two-decay-time fits were

Table 2

Wavelength dependence of the lifetimes of oxyhemoglobin

Wavelengths were selected using interference filters with a 10 nm bandpass.

Wavelength (nm)	τ_i (ns)	α_i	f_i	χ^2_R
315	0.016	0.991	0.72	
	0.463	0.007	0.16	
	3.460	0.001	0.12	3.03/21.28 [b]
322	0.018	0.981	0.60	
	0.501	0.018	0.32	
	4.458	0.001	0.08	2.09/22.66
340	0.018	0.979	0.54	
	0.492	0.019	0.30	
	3.642	0.001	0.16	2.38/54.84
360	0.017	0.972	0.42	
	0.498	0.024	0.30	
	3.950	0.002	0.28	2.58/131.14
380	0.018	0.968	0.37	
	0.500	0.033	0.35	
	3.773	0.003	0.28	3.34/148.43
Global	0.017±0.007	0.992	0.702 [c]	
		0.981	0.572	
		0.979	0.500	
		0.972	0.415	
		0.964	0.376	
	0.486±0.002	0.007	0.143	
		0.018	0.300	
		0.019	0.277	
		0.025	0.305	
		0.033	0.368	
	3.716±0.08	0.001	0.155	2.83/85.16
		0.001	0.128	
		0.002	0.223	
		0.005	0.280	
		0.003	0.256	

[a] In 0.015 M Tris buffer at pH 8.0; approx. 0.03 M sodium acetate, protein concentration 2 g/dl at 4°C. Interference filters with a bandpass of 10 nm were used in the emission path; excitation at 290 nm; front-face geometry.

[b] The second value is the χ^2_R value from the two-decay-time fit.

[c] These are the wavelength-dependent values of $\alpha_i(\lambda)$ and $f_i(\lambda)$, at 315, 322, 340, 360 and 380 nm (from top to bottom).

Table 3

Wavelength dependence of the lifetimes of carbonmonoxyhemoglobin

Wavelengths were selected using interference filters with a 10 nm bandpass.

Wavelength (nm)	τ_i (ns)	α_i	f_i	χ^2_R
315	0.029	0.992	0.78	
	0.839	0.007	0.17	
	3.608	0.005	0.05	1.96/4.19 [b]
322	0.028	0.989	0.76	
	0.612	0.009	0.16	
	3.113	0.001	0.08	1.90/7.91 [b]
340	0.027	0.981	0.64	
	0.643	0.017	0.26	
	3.505	0.001	0.10	2.32/15.127 [b]
360	0.027	0.976	0.59	
	0.596	0.022	0.29	
	4.264	0.001	0.12	2.24/29.24 [b]
380	0.026	0.970	0.52	
	0.533	0.027	0.30	
	4.189	0.002	0.18	2.38/70.16 [b]
Global	0.028 ± 0.0002	0.990	0.744 [c]	
		0.990	0.744	
		0.981	0.742	
		0.977	0.610	
		0.973	0.538	
	0.609 ± 0.001	0.009	0.147	
		0.009	0.147	
		0.018	0.148	
		0.022	0.299	
		0.025	0.301	
	4.067 ± 0.22	0.001	0.109	3.21/674.96 [b]
		0.001	0.109	
		0.001	0.110	
		0.001	0.091	
		0.002	0.161	

[a] In 0.015 M Tris buffer at pH 8.0; approx. 0.03 M sodium acetate, protein concentration 2 g/dl at 4°C. Interference filters with a band-pass of 10 nm were used in the emission path; excitation at 290 nm; front-face geometry.

[b] The second value is the χ^2_R value from the two-decay-time fit.

[c] Wavelength-dependent values of $\alpha_i(\lambda)$ and $f_i(\lambda)$ at 315, 322, 340, 360 and 380 nm (reading downward).

not adequate to account for the data, as can be judged by the approx. 10-fold increase in χ^2_R. Tables 2 and 3 list the lifetime parameters obtained at the various wavelengths, for HbO_2 and HbCO, respectively. When the data at each wavelength were analyzed individually the values of the lifetimes were not significantly dependent upon emission wavelength. This fact was also evident from the global fits to the data measured at all wavelengths. In this case, the decay times were forced to be the same at each wavelength. Since the value of χ^2_R was only slightly elevated for the global fit we conclude that both fits (global and nonglobal) were adequate to describe the data. In both cases, global and nonglobal, the relative proportions of the picosecond and nanosecond lifetimes varied with wavelength. In particular, the intensity of the nanosecond lifetimes increased with wavelength, suggesting a time-dependent shift of the emission to longer wavelength.

We used the impulse response functions from the nonglobal fits to calculate the time-resolved emission spectra of HbO_2 and HbCO (fig. 7). The emission of HbCO appears to occur at longer wavelengths than for HbO_2. At short times blue-shifted spectra are seen, comparable to those found for HbO_2 (fig. 4). At longer times the emission spectrum is comparable to that of apo-Hb. At

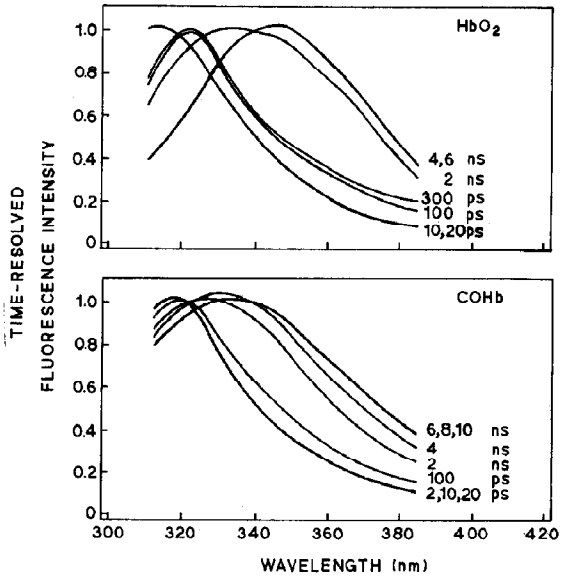

Fig. 7. Time-resolved spectra of HbO_2 (top) and HbCO (bottom). The data were obtained using front-face geometry, in 0.015 M Tris buffer at pH 8.0, approx. 0.03 M sodium acetate, protein concentration 2 g/dl at 4°C.

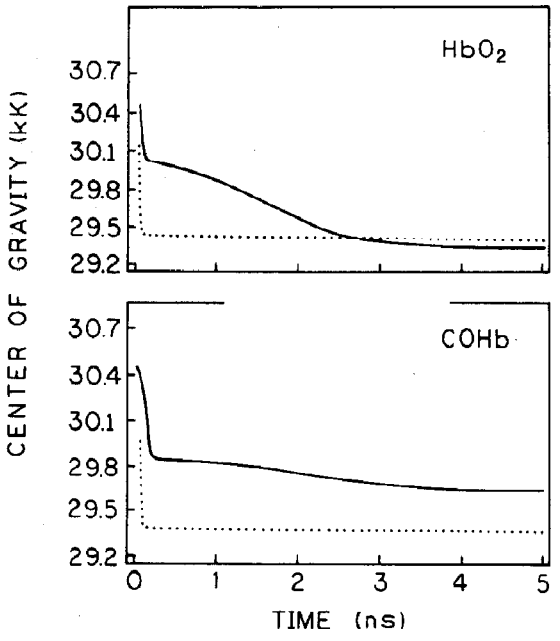

Fig. 8. Time-dependent center-of-gravity of the time-resolved spectra of HbO_2 (upper) and HbCO (lower). Also shown are model calculations (·····) for two separate and noninterchanging emissions, with decay times of 10 ps and 5 ns. Simulated data were calculated as described in the text, using nine wavelengths from 310 to 390 nm. The values of f_1 were 0.63, 0.54, 0.46, 0.40, 0.34, 0.30, 0.28, 0.27 and 0.2, respectively, and $f_1 + f_2 = 1.0$.

intermediate times (300 ps for HbO_2 and 2 ns for HbCO) the emission spectra appear to be wider than at shorter and longer times. This behavior is characteristic of two emitting populations [17].

The time-resolved spectra were characterized further by calculation of the time-resolved centers-of-gravity (fig. 8). The center-of-gravity shows an initial rapid decrease in less than 400 ps, followed by a slower or constant value at longer times. This behavior does not appear to be characteristic of a relaxing system, where the shorter wavelength emission is relaxing to longer wavelengths. Such systems display more gradual and/or exponential-like decays in the emission center-of-gravity. However, this type of behavior is expected for two populations of noninteracting fluorophores, with widely differing decay times and centers-of-gravity. This is shown by model calculations of $\bar{\nu}_{cg}(t)$ using parameter values expected for Hb and impurities. In particular, we assumed a decay time of 10 ps for the Hb emission and 5 ns for the long-wavelength emission. The emission spectra associated with these decay times were assumed to be those of HbO_2 and apo-Hb, respectively (fig. 4). We additionally assumed that the steady-state spectra of HbO_2 and apo-Hb had the same peak intensity, and that the total emission spectrum was the sum of these two spectra. These assumptions allowed calculation of $f_1(\lambda)$ and $f_2(\lambda)$ at each emission wavelength, as depicted in fig. 8. The simulated values of $\bar{\nu}_{cg}(t)$ display a rapid initial decrease, followed by a constant value for several nanoseconds. Hence, the simulated values support the notion that the time-resolved centers-of-gravity observed for HbO_2 and HbCO are the result of emission from two populations of emitting species. We note that we made no attempt to fit the simulated values to the actual data. Also, the lack of agreement at intermediate times is due to the three decay times observed for the Hb samples, while only two decay times were used for the simulations.

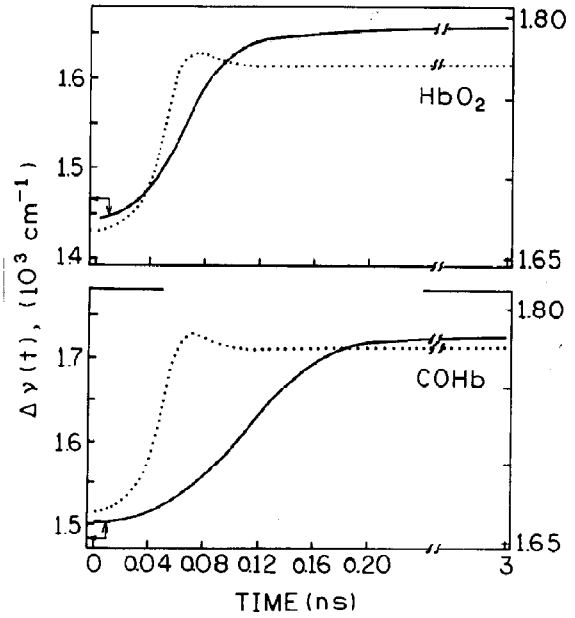

Fig. 9. Time-dependent half-width of the emission spectrum of HbO_2 (top) and HbCO (bottom). Also shown are model calculations for the two emitting populations modeled in fig. 8 (·····), with scaling on the right.

We also calculated the time-resolved half-widths ($\Delta\bar{\nu}_{cg}(t)$, fig. 9) from our experimental data from HbO_2 and HbCO. These half-widths display an initial constant value up to about 40 ps. The half-width then increases until 200 ps and then remains constant. This behavior is also consistent with two separate emitting populations, as can be seen from the model calculations using the same assumptions and parameters as were used for simulations of $\bar{\nu}_{cg}(t)$. The simulated half-width for the two separate populations mentioned above (fig. 9) also displays the region of constancy from 0 to 40 ps. The half-width at short times is close to that found for the picosecond components of the emission. At later times the half-width becomes constant and equal to that of the longer-lived emission. The lack of agreement at intermediate times is not a discrepancy in that the simulated data were for two decay times, whereas the experimental data were obtained from the triple-exponential analysis.

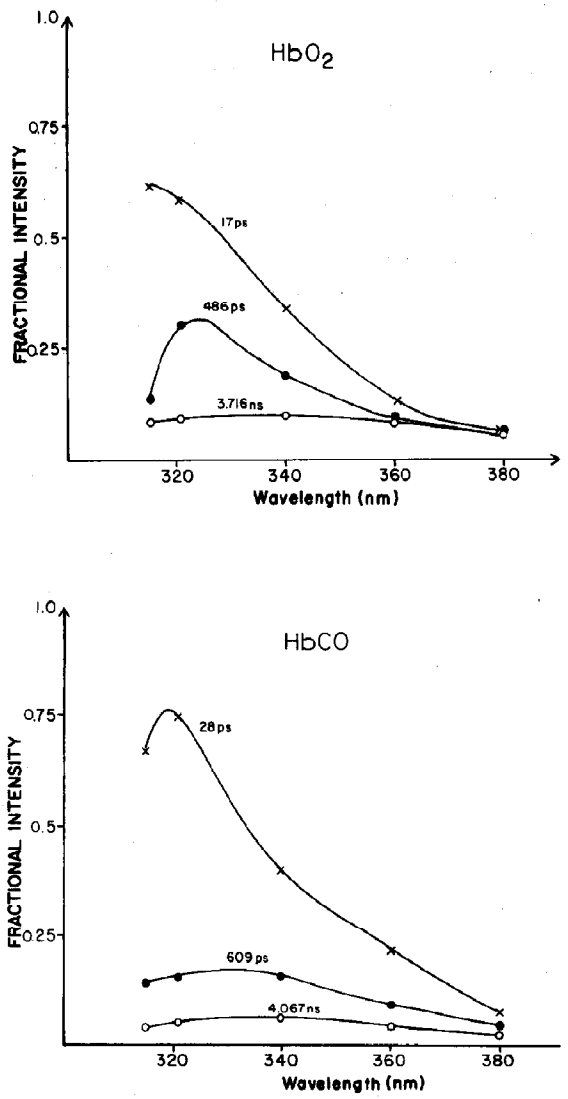

Fig. 10. Decay-associated emission spectra of HbO_2 (top) and HbCO (bottom). These spectra were calculated using eq. 9 and the global analysis results (tables 2 and 3).

An alternative representation of the wavelength-dependent time-resolved data is given by the DAS. These are the emission spectra which are associated with each decay time (fig. 10). These spectra were calculated using eq. 9 and the results from global analysis of the wavelength-dependent data (tables 2 and 3). For both HbO_2 and HbCO the spectrum associated with the picosecond decay time is strongly blue-shifted, with emission maxima near or below 320 nm. The spectra associated with the 0.5–0.7 ns component display intermediate emission maxima, the nanosecond components showing maxima near 340 nm. It should be noted that the dominant emission is associated with the picosecond component, and that the contribution of the nanosecond component is minimal. The low intensities of the nanosecond components do not allow a clear interpretation of their similarity or difference. In total, the time-resolved spectra, centers-of-gravity, half-widths and decay-associated spectra support our argument that the picosecond and nanosecond components are due to separate emitting populations, which do not interchange significantly during the excited-state lifetime.

4. Conclusions

The combination of 2 GHz frequency-domain fluorometry and front-face observation is a potential breakthrough in the study of the picosecond fluorescence of Hb and of hemoproteins in general. The intensity is larger than that obtainable with square geometry, the contributions due to scattered light are minimal, and the measurements may be performed using higher concentrations of

Hb. These characteristics allow measurements of time-resolved spectra, and of lifetimes and correlation times produced by the picosecond emission. It was only by using front-face techniques that it was possible to measure the time-resolved spectra of the emission. As already reported [10] and here confirmed the various Hb derivatives have different picosecond lifetimes. We should now be able to determine whether the picosecond lifetimes can be used for detecting conformational attitudes of the heme in the liganded and unliganded forms of Hb.

At this time interpretation of the lifetimes in the nanosecond range remains uncertain. The amplitudes of the nanosecond components tend to increase with time following sample preparation. This increase is accompanied by a progressive shift of the emission spectra towards the red. For this reason the samples were discarded after 2 days. Also, the relative intensity and spectral distribution of the nanosecond lifetimes appeared to be dependent on the extent of purification of the samples. These characteristics suggest that the nanosecond lifetimes were produced by tryptophan-containing impurities, not quenched by heme, and practically impossible to eliminate. The possibility still exists that improbable conformational attitudes of the tryptophans, which substantially reduce the energy transfer to the heme, are responsible for the nanosecond emission. The 'impurities' might then be slowly relaxing conformers of Hb, which are selectively rejected by the fast chromatographic procedure used for the purification of the samples.

It should be stressed that the emission spectra reported by Hirsch and collaborators [26,27] have emission maxima near 330 nm. This implies an emission which is the result of both the pico- and nanosecond components described above. The sensitivity of the picosecond component to ligation could account for the consistency of the spectral changes with respect to the allosteric behavior of Hb.

Acknowledgements

This work was supported by the following grants: PHS-HL-13164, PHS-HLB-33629 (E.B.), NSF DBM-8511065 and DBM-8502835 (J.R.L.). Computer time and facilities were supported in part by the computer network of the University of Maryland at College Park and its branch at the Baltimore campus. We also acknowledge the use of frequency-domain software developed in the laboratory of J.R.L. under NSF DMB-8511065. The authors also acknowledge the generous support of the Medical Biotechnology Center, University of Maryland.

References

1 A.P. Demchenko, Ultraviolet spectroscopy of proteins (Springer, Heidelberg, 1986).
2 S.V. Konev, Fluorescence and phosphorescence of proteins and nucleic acids (Plenum, New York, 1967).
3 J.R. Lakowicz, Principles of fluorescence spectroscopy (Plenum, New York, 1983) ch. 11, p. 341.
4 J.M. Beechem and L. Brand, Ann. Rev. Biochem. 54 (1985) 41.
5 T. Forster, Ann. Phys. (Leipzig) 2 (1948) 55.
6 G. Weber and F.W.J. Teale, Disc. Faraday Soc. 27 (1959) 134.
7 B. Alpert, D.M. Jameson and G. Weber, Photochem. Photobiol. 31 (1980) 1.
8 A.G. Szabo, D. Krazcarski, M. Zukes and B. Alpert, Chem. Phys. Lett. 108 (1984) 145.
9 R.M. Hochstrasser and D.K. Negus, Proc. Natl. Acad. Sci. U.S.A. 81 (1984) 4399.
10 E. Bucci, H. Malak, C. Fronticelli, I. Gryczynski and J.R. Lakowicz, J. Biol. Chem. 263 (1988) 6972.
11 J. Eisinger and J. Flores, Anal. Biochem. 94 (1979) 15.
12 R.E. Hirsch and J. Peisach, Biochim. Biophys. Acta 872 (1986) 147.
13 R.E. Hirsch and R.W. Noble, Biochim. Biophys. Acta 914 (1987) 213.
14 J.R. Lakowicz, G. Laczko and I. Gryczynski, Rev. Sci. Instrum. 57 (1986) 2499.
15 J.R. Lakowicz, E. Gratton, G. Laczko, H. Cherek and M. Limkeman, Biophys. J. 46 (1984) 463.
16 M.G. Badea, R.P. DeToma and L. Brand, Biophys. J. 24 (1978) 197.
17 J.R. Lakowicz, H. Cherek, G. Laczko and E. Gratton Biochim. Biophys. Acta 777 (1984) 183.
18 J.R. Lakowicz, H. Szmacinski and I. Gryczynski, Photochem. Photobiol. 47 (1988) 31.
19 R.E. Hirsch, R.C. San George and R.L. Nagel, Anal. Biochem. 149 (1985) 415.
20 R.E. Hirsch, N.A. Squires, C. Discepola and R.L. Nagel, Biochem. Biophys. Res. Commun. 116 (1983) 712.
21 J.R. Lakowicz, J. Biochem. Biophys. Methods 2 (1980) 90.
22 J.R. Lakowicz and A. Balter, Photochem. Photobiol. 36 (1982) 125.

23 J.R. Lakowicz, Principles of fluorescence spectroscopy (Plenum, New York, 1983) ch. 5, p. 111.
24 J.R. Lakowicz, B. Maliwal, H. Cherek and A. Balter, Biochemistry 22 (1983) 1741.
25 J.R. Lakowicz, Principles of fluorescence spectroscopy (Plenum, New York, 1983) p. 133.
26 R.E. Hirsch, R.S. Zukin and R.L. Nagel, Biochem. Biophys. Res. Commun. 93 (1980) 432.
27 R.E. Hirsch and R.L. Nagel, J. Biol. Chem. 255 (1981) 1080.
28 P.R. Bevington, Data reduction and error analysis for the physical sciences (McGraw Hill, New York, 1969).
29 J.R. Knutson, D.G. Walbridge and L. Brand, Biochemistry 21 (1982) 4671.
30 J.M. Beechem, M. Ameloot and L. Brand, Chem. Phys. Lett. 120 (1985) 466.